Journal of Photopolymer Science and Technology
Volume 35, Number 1 (2022) 95 −100 ©2022SPST

Influence of Counteranions on the Performance of Tin-based EUV Photoresists

Quentin Evrard[1*], Najmeh Sadegh[1], Yasin Ekinci[2], Michaela Vockenhuber[2] Nicola Mahne[3], Angelo Giglia[3], Stefano Nannarone[3], Tsuyoshi Goya[4], Takuo Sugioka[4], and Albert M. Brouwer[1,5]

[1] Advanced Research Center for Nanolithography, Science Park 106, 1098 XG Amsterdam, The Netherlands
[2] Paul Scherrer Institute, Forschungsstrasse 111, 5232 Villigen PSI, Switzerland
[3]IOM-CNR, Strada Statale 14 km 163,5, 34149 Basovizza-Trieste, Italy
[4] Nippon Shokubai Co., LTD.5-8 Nishi Otabi-cho, Suita, Osaka 564-0034, Japan
[5] University of Amsterdam, van 't Hoff Institute for Molecular Sciences, PO Box 94157, 1090 GD Amsterdam, The Netherlands
**q.evrard@arcnl.nl*

A positive-tone extreme ultraviolet (EUV) photoresist was obtained via the exchange of the hydroxide ions of tin-oxo-hydroxo cages with tetrakis(pentafluorophenyl)-borate. Thin films were obtained after spin coating on silicon substrates and exposed to line patterns in interference lithography at 92 eV (13.5 nm). For low doses and development with ethylbenzene positive tone patterns were obtained. In contrast, the exchange of the hydroxide ions of tin-oxo-hydroxo cages with tetrakis(4-methylphenyl)-borate or tetrakis[3,5-bis(1,1,1,3,3,3-hexafluoro-2-methoxy-2-propyl)phenyl]-borate led to the negative-tone photoresist behaviour that has previously been observed for tin-oxo cages with all other counterions. In situ exposures at 92 eV and subsequent X-ray Photoelectron Spectroscopy were performed on a film of tin-oxo-hydroxo cages with tetrakis(pentafluorophenyl)-borate anions to probe the chemical changes induced by the EUV exposure. This shows that the C-F bonds of the anions are relatively stable.

Keywords: Positive-tone Resist, Tin-oxo-hydroxo Cage, Extreme Ultraviolet Lithography, Inorganic-organic Hybrid Photoresist

1. Introduction

Inorganic molecular materials are of prime interest in the Extreme UltraViolet (EUV) photoresist community [1-4] due to their increased EUV absorption cross section compared to conventional organic-based photoresists. Among these materials tin-oxo-hydroxo cages [5-6] are promising materials. The tin-oxo-hydroxo cages (molecular formula $\{(BuSn)_{12}(\mu_3\text{–}O)_{14}(\mu_2\text{-}OH)_6\}^{2+}$) are positively charged clusters of twelve tin atoms bridged by oxygens and have one butyl group attached to each tin atom forming a layer at the surface of the cluster enhancing its solubility. The bond between the tin atoms and their respective butyl groups is known to be labile when the cages are exposed to electrons [7], UV [8,9], or EUV [10]. A simulation model [11] of this type of photoresist assumes that Sn-C bond breaking generates active sites on the tin atoms that lead to the cross-linking between neighbouring clusters, causing the exposed material to become insoluble.

In earlier work we have observed that the sensitivity and patterning behavior of tin-oxo cages with different small counterions differs somewhat, but not dramatically [6]. To gain more insight into the role of the counterions, in the present work we use large non-nucleophilic tetraphenylborate anions. Indeed, the anion exchange properties of tin-oxo-hydroxo clusters are well documented [12-14] and offer an opportunity to tailor the properties of the resist. One of the main challenges of the hybrid organic-inorganic resists is to further increase their EUV absorption cross-section to generate more active sites per volume of resist and thus potentially

Received March 31, 2022
Accepted June 24, 2022

increase the photoresist sensitivity. To that end, in the present work we introduce fluorinated borate counteranions on the tin-oxo-hydroxo cages. The EUV absorption cross-section of fluorine is 3.5 times higher than that of carbon and 1.3 times higher than that of oxygen. Three anions of interest are discussed in the present work, namely tetrakis(pentafluorophenyl)-borate ($B(PFP)_4^-$) (in **1**), tetrakis(4-methylphenyl)-borate ($B(Tolyl)_4^-$) **(2)** and tetrakis[3,5-bis(1,1,1,3,3,3-hexafluoro-2-methoxy-2-propyl)phenyl]-borate ($B(HFOMePr)_4^-$) **(3)** (see figure 1).

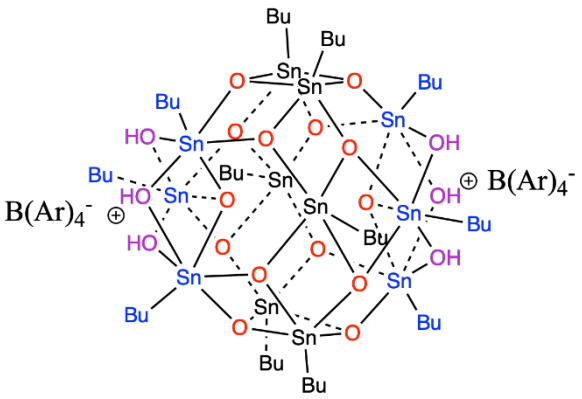

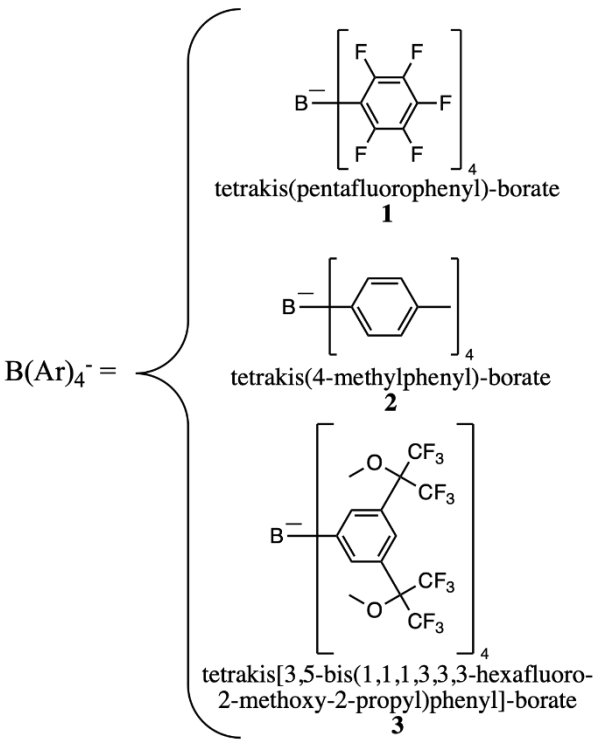

Fig. 1. Structure of the tin oxo-hydroxo cage and counteranions used in this work. TinOH is the same cage with two OH^- counterions.

It is expected that the fluorine content leads to an increase of the EUV absorption of the photoresist film. The lithographic properties of the three materials were studied, and in-situ EUV exposures coupled with X-ray photoelectron spectroscopy have been performed on the $B(PFP)_4$ system **1**.

2. Experimental

2.1. Chemical synthesis

The acid forms of $B(PFP)_4^-$ and $B(Tolyl)_4^-$ are obtained from their sodium salts via the reaction with a slight excess (1.07:1) of aqueous HCl (37%) in water heated at 40°C for 30 minutes. The obtained mixture is extracted with diethylether five times and the aqueous phase is discarded. The organic phase is then allowed to evaporate via heating at 35 °C. The obtained viscous liquid is dispersed in water and sonicated for a further two hours. The dispersion is then cooled down to room temperature, filtered and washed with water three times. The resulting white powder is used without further purification (yield 60 - 70%).

The synthesis of the tin-oxo-hydroxo cage with hydroxide anions (TinOH) is performed as in previous work [9] via the hydrolysis of butyltin-hydroxide-oxide in the presence of p-toluene-sulfonic acid followed by exchange of the toluene-sulfonate for hydroxide counterions using tetramethylammonium hydroxide aqueous (25%) solution. After recrystallization from isopropanol/water (6.5:1), TinOH (250 mg; 0.100 mmol) is dispersed in 4 mL of toluene and mixed with a 10 mL aqueous solution of tetrakis(pentafluorophenyl)-boric acid (136 mg; 0.200 mmol). After 2 hours of vigorous stirring and ultrasonication, the resulting two-phase system is allowed to cool down for two additional hours. The toluene layer is separated, filtered and washed with distilled water (5 mL) three times. The white powder resulting after evaporation of the solvent is used as photoresist material without further purification (yield of **1**: 80%) ^{1}H NMR (400 MHz, $CDCl_3$): For compound **1**: δ = 1.73 (m, Sn_5-C**H₂**-C**H₂**-CH_2-CH_3), 1.44 (m, Sn_5-CH_2-CH_2-C**H₂**-CH_3, Sn_6-CH_2-C**H₂**-CH_2-CH_3), 1.28 (m, Sn_6-CH_2-CH_2-C**H₂**-CH_3, J = 7.2 Hz), 1.14 (m, Sn_6-C**H₂**-CH_2-CH_2-CH_3), 0.97 (t, Sn_5-/-C**H₃** J = 7.3 Hz), 0.85 (t, Sn_6-/-C**H₃** J = 7.3 Hz), 1.73 (m, Sn_5-C**H₂**-C**H₂**-CH_2-CH_3).

For compound **2**: δ = 6.91-7.04 (m, B-[**o-H**Ph-CH_3]$_4$), 6.86 (d, B-[**m-H**Ph-CH_3]$_4$ J = 7.4 Hz), 2.22 (s, B-[Ph-C**H₃**]$_4$), 1.71 (m, Sn_5-CH_2-C**H₂**-CH_2-CH_3, J = 7.3 Hz), 1.39-1.58 (m, Sn_6-CH_2-C**H₂**-CH_2-CH_3

and Sn_5-C**H₂**-CH_2-C**H₂**-CH_3), 1.32 (m, Sn_6-CH_2-CH_2-C**H₂**-CH_3 J = 7.1 Hz), 1.03 (m, Sn_6-C**H₂**-CH_2-CH_2-CH_3) 0.96 (t, Sn_5-/-C**H₃** J = 7.1 Hz), 0.89 (t, Sn_6-/-C**H₃** J = 7 Hz).

For compound **3**: δ = 7.49 (s, B-[C_6H(**o-H**)$_2$ m-($C(CF_3)_2OCH_3$)]$_4$, 7.36 (s, B-[C_6H_2**p-H** m-($C(CF_3)_2OCH_3$)]$_4$, 3.25 (s, B-[C_6H_3 m-($C(CF_3)_2OC$**H₃**)]$_4$, 1.75 (m, Sn_5-CH_2-C**H₂**-CH_2-CH_3), 1.42-1.57 (m, Sn_6-CH_2-C**H₂**-CH_2-CH_3 and Sn_5-C**H₂**-CH_2-C**H₂**-CH_3), 1.35 (m, Sn_5-CH_2-CH_2-C**H₂**-CH_3), 1.25 (m, Sn_6-C**H₂**-CH_2-CH_2-CH_3), 0.97 (t, Sn_5-/-C**H₃** J = 7.3 Hz), 0.89 (t, Sn_6-/-C**H₃** J = 7.3 Hz). (Sn_5 refers to the 6 tin atoms that are 5-coordinated in the tin-oxo-hydroxo cage while Sn_6 refers to the 6 tin atoms that are 6-coordinated)

The anion exchange procedure is identical for the tetrakis(4-methylphenyl)-boric acid. The synthesis of **3** only differs by the use of the sodium salt of the borate instead of its acid form.

2.2. Thin film sample preparation

The photoresist solutions of interest (10 mg/mL) are all prepared using trifluorotoluene as solvent. Following the dissolution, they are sonicated for an additional 10 minutes. The solutions are filtered using a 0.20 µm PTFE filter and directly spincoated.

All samples for EUV lithography were prepared on silicon wafers (Siegert Wafer, CZ growth, p-type B-doped, <100>, resistivity 5-10 Ohm-cm) used without further cleaning. The spin coating is done with a rotation speed of 2000 rpm, an acceleration of 750 rpm/s and no post-application or post-exposure baking are performed. The thickness of the obtained films using this procedure is 30-35 nm.

All the samples for in-situ EUV exposures with XPS spectroscopy were prepared on gold-coated Si substrates. The silicon wafer (Siegert Wafer, CZ growth, p-type B-doped, <100>, resistivity 5-10 Ohm-cm) is first diced in 25 × 25 mm substrates. The substrates are cleaned with an 80°C base piranha solution for 15 minutes, rinsed with isopropanol and dried with nitrogen flow. They are then cleaned using an ozone plasma (Diener Electronic Pico QR-200-PCCE) with a two-minute oxygen plasma at 0.2 mbar working pressure. Next, the samples are coated with a gold layer using a sputter coater (Leica EM ACE600 double sputter coater) depositing a 5 nm layer of chromium as adhesion layer followed by 30 nm of gold. The gold-coated substrates are used for spin-coating of the resist solutions, with a rotation speed of 2500 rpm and an acceleration of 750 rpm/s. No pre- or post-exposure baking is performed.

Atomic Force Microscopy is performed on a Bruker Dimension Icon using tapping mode with Bruker TESP-SS tips (320 kHz, 42 N/m), fields of 3 × 0.6 µm were measured with 256 samples per line and a scanning frequency of 0.6 Hz. Raw data was corrected by truncated mean method and flattened by mean plane. No further corrections were made.

3. Results and discussion

3.1. Strategy

In TinOH, most of the EUV absorption originates from the tin atoms present in the tin oxo-hydroxo cage [15]. The replacement of the small OH^- with larger organic anions leads to a decrease of EUV absorption of the photoresist because the number of strongly absorbing tin atoms per unit volume is reduced, while the organic anions themselves have only small cross sections at 92 eV. When heavily fluorinated anions are used, the larger cross sections of fluorine will offset the loss of EUV absorption cross section due to dilution of tin. For a thin film of **1** we estimate that the absorption at 92 eV is in fact ~30% higher than that of TinOH.

The non-fluorinated samples prepared from tolylborate **2** are used as reference to investigate the system behaviour when the tin cages are diluted by large low absorption borate counteranions.

3.2. EUV Interference lithography

The EUV lithographic properties of all three photoresists have been studied at the Paul Scherrer Institute (Switzerland) on the XIL-II beamline and line/space patterns have been obtained as exemplified in figure 2.

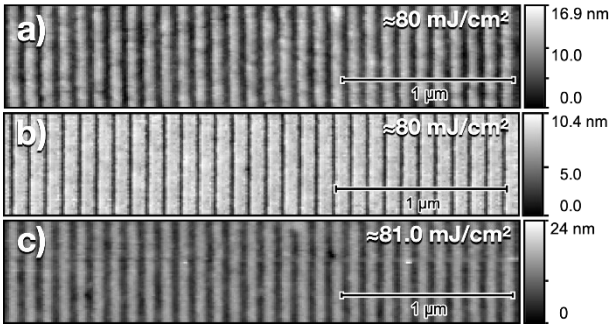

Fig. 2. Atomic force microscopy height images obtained for films of **1** (a), **2** (b) and **3** (c) exposed to EUV irradiation (Line-space patterns with 50 nm half-pitch) and developed with ethylbenzene ((a) and (b)) or n-hexane (c).

All the photoresist samples have been prepared from solutions in trifluorotoluene. A hexamethyldisilazane (HMDS) adhesion promoting layer was necessary to form good quality films with

the non-fluorinated **2**. The developer chosen for **1** and **2** is ethylbenzene. Chemical contrast for **3** could be obtained by using n-hexane. The EUV exposure doses required to see pattern formation are close to 30 mJ/cm^2 for **1** and **2** while higher doses of around 80 mJ/cm^2 are required for **3**. The lowest sensitivity is found for **3**, which has the largest anion. For tolylborate **2** the sample exposed to 80 mJ/cm^2 of EUV irradiation already exhibits signs of overexposure such as decrease of thickness in the middle of the exposed parts due to further material degradation.

While both **2** and **3** exhibit the commonly found negative tone photoresist behaviour of tin-oxo cages, **1** can be developed as a positive tone photoresist for doses ranging from 30 to around 100 mJ/cm^2. The positive tone behaviour of **1** is identified by the widening of the grooves upon increasing the EUV dose. At higher doses the tone inverts to negative, resulting in a complete loss of pattern at intermediate doses. In comparison, the tolylborate **2** exhibits negative tone traits such as increase of line width at doses from 20 to 150 mJ/cm^2 combined with signs of overexposure appearing from 80 mJ/cm^2 and up with a decrease of the line height at its center due to further degradation of the resist on the highest intensity part of the exposed pattern.

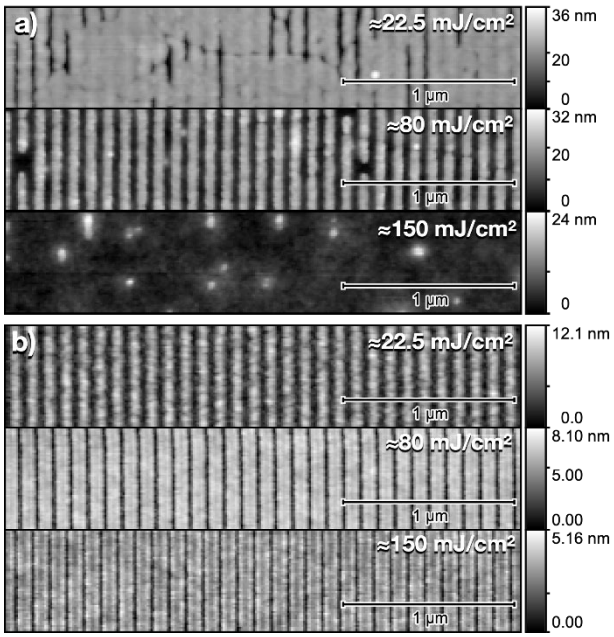

Fig. 3. Atomic force microscopy height images obtained for films of **1** (a) and **2** (b) exposed to EUV irradiation (Line-space patterns with 50-nm half-pitch) and developed with ethylbenzene.

3.3. In-situ EUV exposures with XPS

To get more insight into the behavior of the highly fluorinated tin-oxo cage **1** we performed X-ray Photoelectron Spectroscopy (XPS) on films exposed to EUV irradiation in-situ. These experiments were carried out at the IOM-CNR BEAR beamline at the Elettra Synchrotron (Trieste, Italy). The samples of **1** were prepared as described in section 2.2 on gold substrates to mitigate charging effects. The sample is first exposed to a known dose of EUV irradiation and then C-edge XPS is performed. The photon energy of the probing beam hitting the grounded sample is 400 eV and experimental parameters are adapted to avoid sample degradation during the XPS measurements. To increase the signal/noise ratio, all measurements are done three times on different sample positions and averaged. Selected spectra are shown in figure 4.

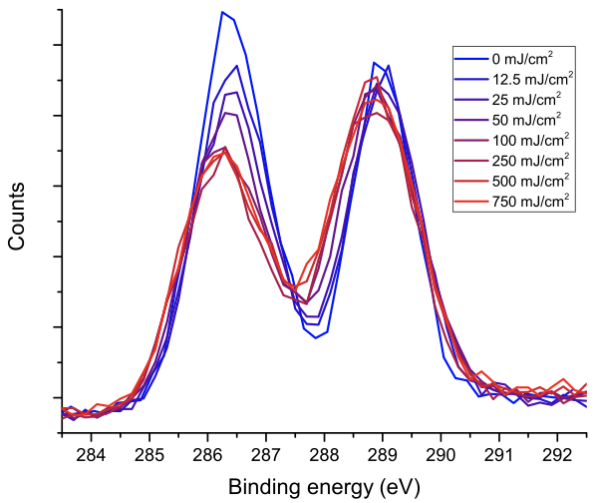

Fig. 4. Evolution of C-edge XPS spectra of bis(tetrakis(pentafluorophenyl)borate) tin-oxo cage **1** upon EUV exposure.

The peak at a binding energy of 289 eV corresponds to the C-F carbons present in the anion and appears to remain mostly unaffected by EUV radiation, while the area of the peak at 286.5 eV that corresponds to the carbons of the butyl chains of the tin-oxo-hydroxo cage is reduced by 30% upon EUV exposure of 250 mJ/cm^2 which is an indication that the butyl groups are outgassed in the high vacuum of the experimental chamber.

3.4. Discussion

The negative tone patterning of **2** and **3** is in line with the known behaviour of tin oxo-hydroxo cage systems. The tin-oxo cage **1**, with the fully fluorinated borate counterion, exhibits positive tone

behaviour over a wide range of doses. Positive tone behaviour has been observed for TinOH under e-beam exposure [16] but only at very small conversion, at which the patterns were too thin to be significant for application. The size of the anion on its own is ruled out as an explanation for this reactivity difference, because the anions in **1** and **2** have similar sizes so have the same effect on the distance between neighbouring tin clusters. The conversion leading to solubility switching of previously studied tin oxo-hydroxo clusters is initiated by the cleaving of Sn-C bonds upon EUV exposure. For the bare tin cage dication this leads to a structure rearrangement, but when a counterion is present, this can form a bond to a tin atom that has lost its organic group [9]. Subsequent cross-linking of neighbouring tin clusters, further enhanced by post-exposure baking [6], is likely to be responsible for the loss of solubility of the exposed material in the negative tone operation. In the present system, the direct cross-linking between neighbouring clusters is inhibited by the steric hindrance of the anions, but the anions are also non-nucleophilic, and less likely than hydroxide, or acetate, to form a bond to a tin atom of the cage.

The reactivity to irradiation of the anion itself can also play a role in the photoresist behavior. Studies of EUV reactivity of aryl-borate molecules have, to the best of our knowledge, not yet been reported although several examples of photolysis [17-18] or photo-induced single electron transfers [19] are present in the literature. Highly fluorinated tetraphenyl borates are much more difficult to oxidize, but at high positive potentials they are electrochemically unstable and can lead to the formation of biphenyl species upon oxidation [20].

The in-situ XPS analysis of **1** indicates that 30% of the butyl chains of the tin-oxo-hydroxo cage are lost upon EUV exposure of 250 mJ/cm^2. Interestingly, an analogous tin-oxo-hydroxo cage cluster with acetate anions exposed to the same EUV doses exhibit a loss of 40% of peak area, pointing towards a reduced reactivity of the tin cluster **1** with the fluorinated tetraphenylborate anion. This could be due to this borate anion acting as a relatively unreactive EUV absorber inhibiting the Sn-C bond cleavage of the tin cluster. Another hypothesis is that the polymerization of several clusters might also favour the cleaving of additional Sn-C bonds next to the bridging oxygen but there is no evidence to rule out either hypothesis. The XPS peak stemming from the carbons linked to fluorine of **1** is slightly broader with a FWHM increasing from 1.28 eV to 1.82 eV during exposure which could indicate a modification of the chemical environment of the pentafluorophenyl groups or the formation of decomposition products with similar binding energies which remain inside the film. Further studies are being conducted on the fluorinated system **1** to gather more evidence on the reaction pathway leading to the solubility switch.

4. Conclusion

Three new photoresists derived from tin-oxo-hydroxo clusters have been synthesized, namely **1** (with $B(PFP)_4$ counterions), **2** (with $B(Tolyl)_4$) and **3** (with $B(HFOMePr)_4^-$). These photoresists all exhibit chemical contrast upon EUV exposure and development but while both **2** and **3** show the usual negative tone photoresist behaviour, **1** can be developed as a positive tone photoresist. In-situ XPS measurements have been performed on **1** and indicate the loss of butyl groups upon EUV exposure while the pentafluorophenyl groups of the anion mostly remain in the film.

Acknowledgement

Part of this work has been carried out within ARCNL, a public–private partnership between UvA, VU, NWO, and ASML. The project has received funding from the European Union's Horizon 2020 research and innovation programme under the Marie Skłodowska-Curie grant agreement No 722149. Synchrotron beam time was provided by the Paul Scherrer Institute where the interference lithography experiments were carried out (proposal 20200726) and the Sincrotrone Elettra (Trieste, Italy) where in-situ XPS experiments were performed (proposal 20205228) Part of this work was supported by Nippon Shokubai.

References

1. M. E. Krysak, J. M. Blackwell, S. E. Putna, M. J. Leeson, T. R. Younkin, S. Harlson, K. Frasure, and F. Gstrein, *Proc. SPIE*, **9048** (2014) 904805.
2. Z. Wang, X. Yao, H. An, Y. Want, J. Chen, S. Wang, X. Guo, T. Yu, Y. Zeng, G. Yang, and Y. Li, *J. Microelectron. Manuf.*, **4** (2021) 21040101.
3. S. Kataoka and K. Sue, *Eur. J. Inorg. Chem.*, **12** (2022) e202200050.
4. M. Murphy, N. S. Upadhyay, M. Ali, J. Passarelli, J. Grzeskowiak, M. Weires, and R. L. Brainard *J. Photopolym. Sci. Technol.*, **34** (2021) 117.
5. B. Cardineau, R. Del Re, M. Marnell, H. Al-

Mashat, M. Vockenhuber, Y. Ekinci, C. Sarma, D. A. Freedman, and R. L. Brainard, *Microelectron. Eng.*, **127** (2014) 44.
6. J. Haitjema, Y. Zhang, M. Vockenhuber, D. Kazazis, Y. Ekinci, and A. M. Brouwer, *J. Micro/Nanolith. MEMS MOEMS*, **16** (2017) 033510.
7. I. Bespalov, Y. Zhang, J. Haitjema, R. M. Tromp, S. J. van der Molen, A. M. Brouwer, J. Jobst, and S. Castellanos, *ACS Appl. Mater. Interfaces*, **12** (2020) 9881.
8. Y. Zhang, J. Haitjema, X. Liu, F. Johansson, A. Lindblad, S. Castellanos, N. Ottosson, and A. M. Brouwer, *J. Micro/Nanolith. MEMS MOEMS*, **16** (2017) 023510.
9. J. Haitjema, L. Wu, A. Giuliani, L. Nahon, S. Castellanos, and A. M. Brouwer, *Phys. Chem. Chem. Phys.*, **23** (2021) 20909.
10. J. Haitjema, L. Wu, A. Giuliani, L. Nahon, S. Castellanos, and A. M. Brouwer, *J. Photopolym. Sci. Technol.*, **31** (2018) 243.
11. W. D. Hinsberg and S. Meyers, *Proc. SPIE*, **10146** (2017) 1014604.
12. C. Eychenne-Baron, F. Ribot, and C. Sanchez, *J. Organomet Chem.*, **567** (1998) 137.
13. F. Ribot, E. Banse, E. Diter, and C. Sanchez, *New J. Chem.*, **19** (1995) 1145.
14. F. Ribot, C. Sanchez, R. Willem, J. C. Martins, and M. Biesemans, *Inorg.Chem.*, **37** (1998) 911.
15. R. Fallica, J. Haitjema, L. Wu, S. Castellanos Ortega, A. M. Brouwer, and Y. Ekinci, *J. Micro/Nanolith. MEMS MOEMS*, **17** (2018) 023505.
16. Y. Zhang, J. Haitjema, M. Baljozovic, M. Vockenhuber, D. Kazazis, T. A. Jung, Y. Ekinci, and A. M. Brouwer, *J. Photopolym. Sci. Technol.*, **31** (2018) 249.
17. J. L. R. Williams, J. C. Doty, P. J. Grisdale, R. Searle, T. H. Regan, G. P. Happ, and D. P. Maier, *J. Am. Chem. Soc.*, **90** (1968) 53.
18. P. J. Grisdale, J. L. R. Williams, M. E. Glogowski, and B. E. Babb, *J. Org. Chem.*, **36** (1971) 544.
19. S. T. Murphy, C. Zou, J. B. Miers, R. M. Ballew, D. D. Dlott, and G. B. Schuster, *J. Phys. Chem.*, **97** (1993) 13152.
20. S. B. Beil, S. Mohle, P. Endersa, and S. R. Waldvogel, *Chem. Commun.*, **54** (2018) 6128.